



JOINT INSTITUTE FOR NUCLEAR RESEARCH
Flerov Laboratory of Nuclear Reactions

# *Overview of the DGFRS-2 Gas-Filled Recoil Separator and Development of Diagnostic Visualization Software for Its DAQ System*

**Supervisor:**
Dr. Vladimir Utyonkov

**Student:**
Ege Can Karanfil
Ankara University, Institute of Nuclear Sciences, Türkiye

**Participation period:**
October 05 –November 29,
Summer Session 2025

Dubna, 2025

# Table of Contents

## Abstract

In this work, DGFRS-2 Gas-Filled Recoil Separator and its design parameters are studied and two complementary software tools were developed to enable fast data processing and provide basic analysis for the DGFRS-2 detector system. The first tool parses the binary list-mode output of the Pixie-16 modules and converts it into ROOT format, providing reduced data size and a structured format suitable for further analysis. The second tool offers a user friendly graphical interface for loading calibrated ROOT data, applying detector mapping and calibration parameters, generating coincidence and anticoincidence spectra, and visualizing detector hit distributions. The software was validated using calibration data obtained from the $^{nat}$Yb($^{48}$Ca, 3-5n)$^{215–217}$Th reaction, confirming correct decoding, calibration, and visualization performance.


# 1. Introduction

Study of the superheavy elements (SHE) have opened new scientific questions regarding the limits of nuclear and atomic structure, including whether nuclei even heavier than those currently known can exist and if the “Island of Stability” represents the final boundary on the Chart of Nuclides. Researchers also investigate whether SHE could be produced through natural nucleosynthesis like other long-lived heavy elements, how their electrons behave under extremely strong Coulomb fields, and is their chemical properties remain comparable to those of their lighter homologues. ultimately seeking to determine the true limit of the periodic table [1,2].

In practice, the method for synthesizing and investigating heavy atoms with atomic numbers above $Z \approx 100$ is the production of evaporation residues (EVRs) through heavy-ion–induced complete fusion reactions, followed by their separation using gas-filled recoil separators [3,4]. The first experimental setup dedicated to exploring the superheavy element region at FLNR was the Dubna Gas-Filled Recoil Separator DGFRS-1 installed at the U400 cyclotron in 1989. Using DGFRS, fusion reactions of $^{48}$Ca projectiles with actinide targets enabled the discovery of the heaviest isotopes of Nihonium (Nh, $Z$=113) and five new superheavy elements from Flerovium (Fl, $Z$=114) to Oganesson (Og, $Z$=118), as well as the study of decay properties for more than 50 new isotopes of elements ranging from Rf to Og [5].

The production of isotopes of the heavier elements Z=119 and Z=120, using the heaviest currently available target materials ($^{248}$Cm, $^{249}$Bk, $^{251}$Cf), require higher-Z projectiles such as $^{50}$Ti, $^{51}$V, and $^{54}$Cr. Since the location of the predicted center of stability for spherical superheavy nuclei, which defined by the yet-uncertain proton and neutron magic numbers remains an open question, studying the properties of the isotopes of these elements is crucial for identifying those shell closures [5,6].

Because fusion reactions involving such heavier projectiles are expected to yield significantly lower production cross-sections than those induced by $^{48}$Ca, it is essential to enhance the overall efficiency of experiments. Thus, a new advanced research complex, the Superheavy Element Factory, has been developed at FLNR, JINR [5]. The new gas-filled separator DGFRS-2, featuring enhanced transmission of complete-fusion evaporation residues (ERs) and improved suppression of background particles, is installed on one of the five beam lines of the DC-280 cyclotron.

In DGFRS-2, the identification of synthesized nuclei is carried out after their implantation into position-sensitive detectors by analyzing time, energy, and position correlations between the evaporation residues (ERs) and their subsequent chains of α decays. The signals from the position-sensitive double-sided silicon strip detectors (DSSD, BB-17) are first fed into charge-sensitive preamplifiers (MESYTEC GmbH & Co.), the preamplifier outputs are split into analog and digital processing branches for different uses.

The analog system is primarily used for beam interruption (beam-off mode) upon detecting a correlated sequence of events. Meanwhile, the digital data acquisition is dedicated to detailed decay spectroscopy of superheavy nuclei and is built on XIA Pixie-16 modules. These modules have 16-channel digital pulse processors operating at 100 MHz with 14-bit resolution. A total of seventeen modules are installed at two PXI crates to process signals from the silicon detector array and multi-wire proportional counters (MWPCs) [5,7].

In this study, a software tool was developed to enable rapid data visualization during data acquisition and to verify calibration parameters of the detectors installed at DGFRS-2. The software processes list-mode data obtained from the Pixie-16 modules and extracts pulse heights (energy values) together with timestamps. The extracted data is then visualized in a way that additionally enables coincidence and anticoincidence analysis, supporting rapid evaluation of detector performance and event correlations.

# 2. Systems of the DGFRS-2

Schematic of the DGFRS-2 is shown in Figure 1. It is in the form $Q_vD_hQ_hQ_vD$ where D denotes a dipole magnet, $D_v$, $D_h$ and $D_{vh}$ are dipole magnets focusing in the vertical, horizontal and both directions, respectively. Similarily, $Q_h$ and $Q_v$ mean horizontally and vertically focusing quadrupole lenses respectively [5].

DGFRS-2 operates with hydrogen as the working gas, and a windowless differential pumping system is employed to maintain high vacuum conditions in the beamline while separating it from the gas-filled separator region. The detector module itself is isolated from the hydrogen environment by a thin 0.7 μm Mylar entrance window. Configuration of the DGFRS-2 is shown in Figure 1.

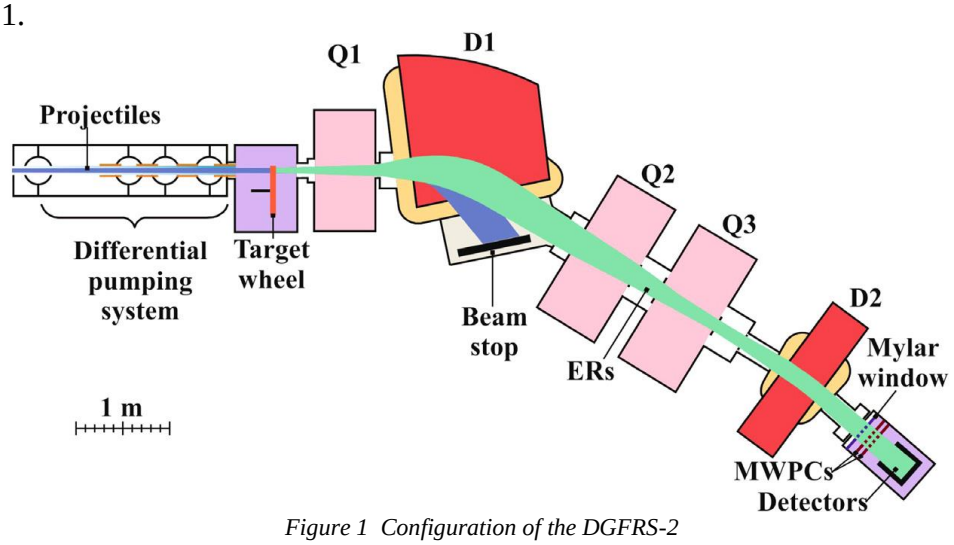


*Figure 1 Configuration of the DGFRS-2*

## 2.1. Target

The target is designed as a rotating disk (target wheel), with the irradiated material mounted on segments along its periphery. Rotation ensures that the deposited beam power and accumulated dose are distributed over a substantially larger area, preventing thermal damage and increasing target lifetime. The DGFRS-2 target wheel, with a diameter of 24 cm, can operate at rotation frequencies of up to 1000 rpm.

To monitor the target condition, periodic measurements of the α-particle counting rate emitted from the irradiated target layers are performed. For this purpose, the magnetic field settings are temporarily adjusted to transport the α-particles toward the focal-plane detector, where the counting rate for each segment is measured without interrupting the continuous rotation of the wheel [5]. The $^{242}$Pu target with 24 cm rotating wheel consisting of 12 double sectors is shown in Fig 2.

*Figure 2 $^{242}$Pu target with 24 cm rotating wheel[5]*

## 2.2. Detector Module

The detector module of DGFRS-2 consists of two multi-wire proportional chambers (MWPCs) and a set of position-sensitive silicon detectors (Fig. 3). In the focal plane, 300-μm-thick double-sided silicon strip detectors (DSSD) are employed. Each DSSD contains 1-mm-wide strips, arranged as 48 horizontal strips on the front side and 128 vertical strips on the back side. Surrounding the focal-plane detectors, eight 500-μm-thick side silicon detectors are installed to register escaping α particles and fission fragments[5].

The detector module is filled with pentane gas at a pressure of 1.6 mbar. The two MWPCs are positioned 65 mm apart downstream of the entrance window, and their signals are utilized to identify the implantation of evaporation residues (ERs) into the silicon detectors. This configuration enables reliable discrimination between beam-related implantation events and the subsequent radioactive decays of implanted nuclei[5].

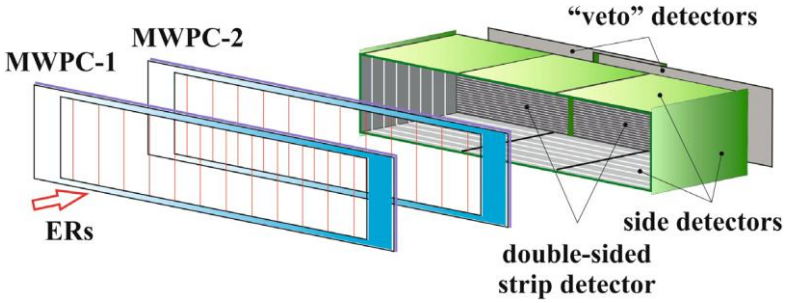


*Figure 3 Detector module of the DGFRS-2[5]*

# 3. Material and Method

## 3.1. Pixie-16 List Mode Data Structure

The detected events are recorded by the Pixie-16 modules in the List Mode data format. In the list-mode data structure, each event begins with a mandatory 4-word (32-bit per word) header that contains essential information such as the event identifier, timestamp, energy value, and trace length. Following this fixed header, additional optional data blocks may appear, depending on the acquisition settings selected by the user. The components of the data structure that are relevant to this study are presented in Figure 4.

| Index | Data (32bit words) | | | | | |
|---|---|---|---|---|---|---|
| 0 | [31] | [30:17] | [16:12] | [11:8] | [7:4] | [3:0] |
| | Finish Code (1 if piled up) | Event Length (32bit words) | Header Length (32bit words) | CrateID | SlotID | Chan# |
| 1 | [31:0] | | | | | |
| | EVTTIME_LO[31:0] | | | | | |
| 2 | [31:16] | | | [15:0] | | |
| | CFD Result [15:0] | | | EVTTIME_HI[15:0] | | |
| 3 | [31] | [30:16] | | [15:0] | | |
| | Trace Out-of-Range Flag | Trace Length (in samples or 16bit words) | | Event Energy | | |

*Figure 4 List mode data structure*

## 3.2. Calibration Reaction

The data used in this study were acquired during the detector calibration measurements. The calibration was performed using the α-particle energies emitted from the reaction products of the $^{nat}$Yb($^{48}$Ca, 3-5n)$^{215–217}$Th reactions. Since the production cross section of these nuclei is on the order of millibarns, the yield is sufficiently high for reliable calibration measurements [5,8,9]. The α-decay spectra of these nuclei and their daughter products are well established in the literature, with the maximum α-particle energy reaching 9.260±0.004 MeV for the $^{217}$Th isotope[10], which has the same order of magnitude with the α-decay energies expected from superheavy nuclei. The other α-particle energies used in the calibration is shown in Table 1.

*Table 1 Alpha-particle energies used for the calibration [9,10]*

| **Isotope** | **$^{210}$Rn** | **$^{208}$Rn** | **$^{212}$Rn** | **$^{212}$Ra** | **$^{214}$Ra** | **$^{216}$Th** | **$^{215}$Ra** | **$^{217}$Th** |
|---|---|---|---|---|---|---|---|---|
| **α-particle energy [keV]** | 6041±3 | 6140.1± 1.7 | 6264±3 | 6899.2 ±1.7 | 7137±3 | 7921 ±5 | 8700± 5 | 9260± 4 |

## 3.3. Decoding and Analysis of the Data

In this work, the raw binary list-mode output of the Pixie-16 modules is converted into ROOT format primarily to achieve a highly efficient data storage structure and significantly reduce overall file size, which is essential for handling large-scale experimental datasets obtained in long superheavy-element experiments. During this conversion, the hardware-encoded event information is decoded, the relevant physical parameters such as energy, timestamp, and channel are extracted, and the events are organized into a structured format. This ROOT-based data model enables fast access, selective reading, event grouping, and histogramming, providing the foundation for subsequent analysis and real-time visualization. The flow-chart of the data decoding algorithm is presented in the Fig. 5.

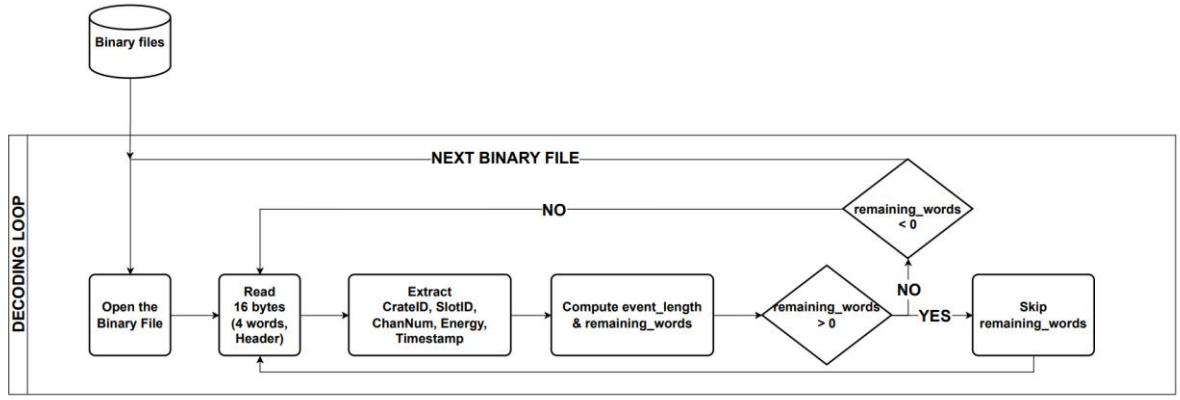


*Figure 5 Flow chart of the data decoding algorithm*

In the developed GUI, the user can select the calibration files, channel/strip mapping, and ROOT files for the data. After loading the required configuration, the ROOT list-mode files are read and merged, and the events are sorted by timestamp. The software then groups the events within a predefined coincidence window and classifies each group as coincidence or anticoincidence depending on the presence of a trigger signal. For each valid hit, channel mapping and calibration parameters are applied to convert ADC values into physical energy units. Finally, calibrated hit information is stored, histograms are generated in multiple categories, and the results are visualized in real time through the GUI. Flowchart of the analysis algorithm and GUI is presented in the Fig. 6.

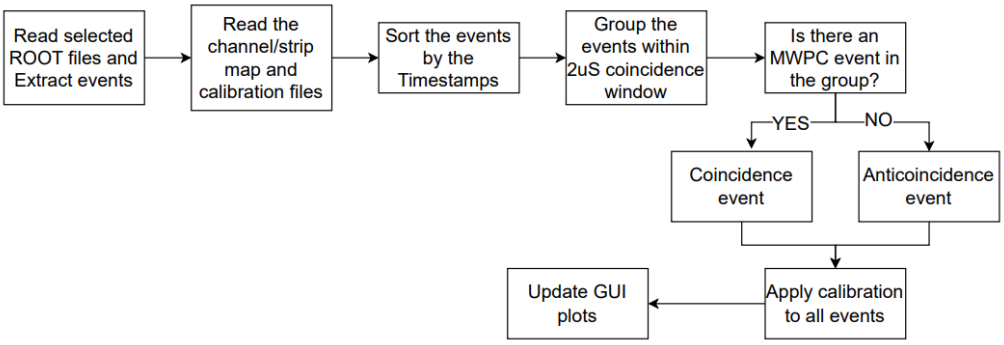


*Figure 6 Flowchart of the analysis algorithm and GUI*

# 4. Results

## 4.1. Overview of the GUI

In the main window of the GUI, two primary buttons are provided. The first button, "Config & Calibration," opens the Configuration Manager (labeled as 2 in Fig. 7), where the user can load mapping and calibration files and define the number of bins for the histograms. Once saved, these settings are automatically stored in a configuration file, eliminating the need to reconfigure the parameters at every startup. The second button allows the user to select the required ROOT files. After the files are chosen, the software automatically performs calibration, processes the events, and generates the corresponding histograms. Switching between coincidence and anticoincidence display modes causes the plots to refresh accordingly. All executed operations are recorded in the Logbook panel located on the left side of the main GUI. Additionally, the bottom section of the main window (labeled as 3 in Fig. 7) provides tools for zooming and panning within the histograms; any change in the viewing range of one plot is immediately synchronized across all histograms to maintain a consistent energy scale.

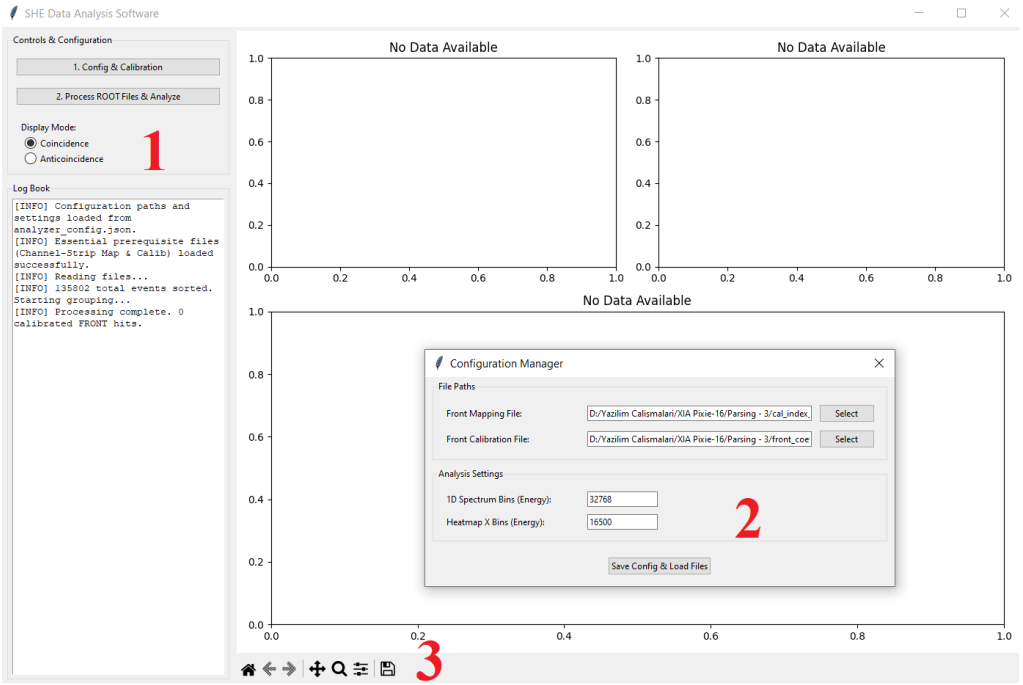


*Figure 7 Main window and the Configuration Manager of the GUI*

The mapping file consists of four columns, which specify the hardware-to-detector correspondence: Crate ID, Slot ID, Channel ID, and Strip ID. These values are used to identify the physical strip of the DSSD to which each electronic channel belongs. Similarly, the calibration file contains four columns defining the linear energy calibration parameters and their uncertainties: Gain, Gain Uncertainty, Offset, and Offset Uncertainty. The gain and offset are applied to convert the ADC values into energy units using a linear relation, while their uncertainties are stored for potential use in error analysis.

## 4.2. Software Tests with the Calibration Data

The data obtained during the $^{nat}$Yb($^{48}$Ca, 3-5n)$^{215–217}$Th calibration reaction were used to test the software. When the decoded ROOT files are loaded into the system, the main GUI appears as shown in Fig. 8. As illustrated, the Logbook reports the total number of processed events as well as the counts of coincidence and anticoincidence events. The displayed histograms include the total (sum) spectrum, the coincidence spectrum, and a two-dimensional Energy vs. Strip heatmap for visualizing the detector hit distribution.

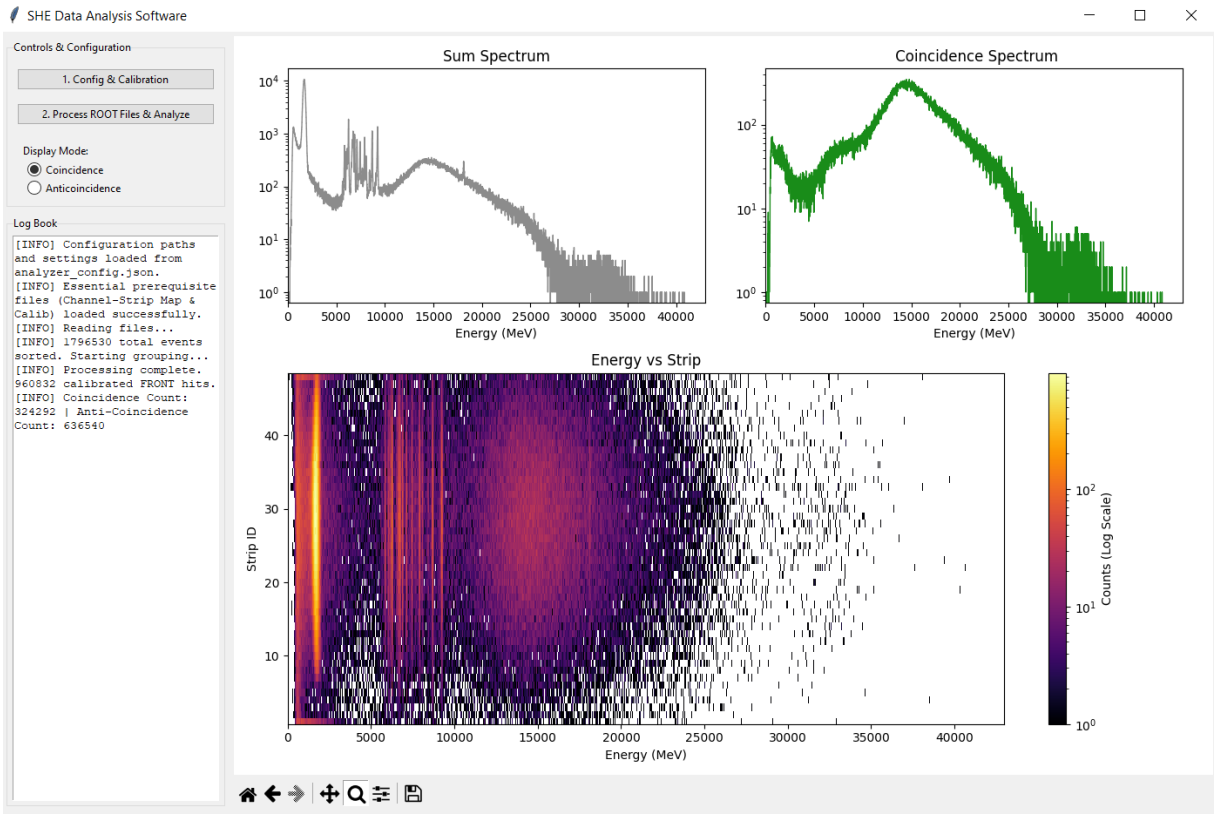


*Figure 8 Test of the analysis and display software with the calibration data*

In Fig. 9, several α-particle energies obtained from the calibration reaction are presented with their corresponding isotopes. These labeled peaks, such as those from $^{217}$Th, indicate the reference energies used in the detector calibration.

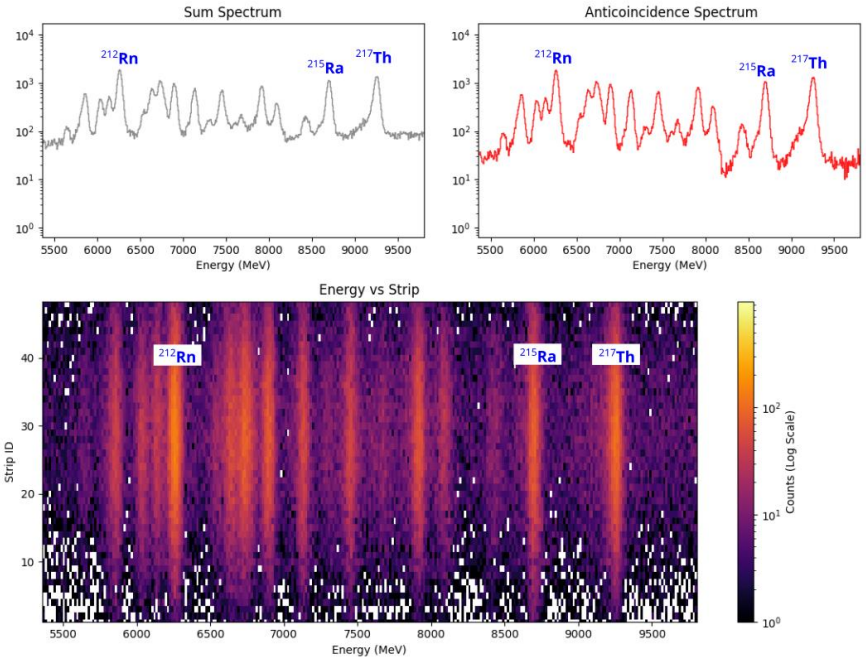


*Figure 9 Labeled α peaks used for the energy calibration.*

# References


[1] Dmitriev S, Itkis M, Oganessian Y. Status and perspectives of the Dubna superheavy element factory. EPJ Web Conf 2016;131:08001. https://doi.org/10.1051/epjconf/201613108001.

[2] Oganessian YT, Utyonkov VK. Super-heavy element research. Reports on Progress in Physics 2015;78:036301. https://doi.org/10.1088/0034-4885/78/3/036301.

[3] Subotic K, Oganessian YuT, Utyonkov VK, Lobanov YuV, Abdullin FS, Polyakov AN, et al. Evaporation residue collection efficiencies and position spectra of the Dubna gas-filled recoil separator. Nucl Instrum Methods Phys Res A 2002;481:71–80. https://doi.org/10.1016/S0168-9002(01)01367-5.

[4] Oganessian YuTs, Utyonkov VK, Lobanov Yu V., Abdullin FSh, Polyakov AN, Shirokovsky I V., et al. Average charge states of heavy atoms in dilute hydrogen. Phys Rev C 2001;64:064309. https://doi.org/10.1103/PhysRevC.64.064309.

[5] Oganessian YuTs, Utyonkov VK, Popeko AG, Solovyev DI, Abdullin FSh, Dmitriev SN, et al. DGFRS-2—A gas-filled recoil separator for the Dubna Super Heavy Element Factory. Nucl Instrum Methods Phys Res A 2022;1033:166640. https://doi.org/10.1016/j.nima.2022.166640.

[6] Oganessian YuTs, Utyonkov VK, Abdullin FSh, Dmitriev SN, Ibadullayev D, Itkis MG, et al. Investigation of reactions with Ti-50 and Cr-54 for the synthesis of new elements. Phys Rev C 2025;112:014603. https://doi.org/10.1103/k2g4-5k7x.

[7] XIA LLC. Pixie-16 User Manual. 2019.

[8] Sagaidak RN, Chelnokov ML, Chepigin VI, Gorshkov VA, Malyshev ON, Popeko AG, et al. Production of evaporation residues in the O-16+Pb-208 and Ca48+Yb-176 reactions. Phys Rev C 2022;105:024604. https://doi.org/10.1103/PhysRevC.105.024604.

[9] Kovrizhnykh ND. Study of the radioactive properties of nuclei in the decay chains of Mc isotopes and the cross sections of their production in the ^{243}Am + ^{48}Ca reaction. JINR, 2024.

[10] National Nuclear Data Center. Evaluated Nuclear Structure Data File 2005.